

Review

A Review of Irradiation-Tolerant Refractory High-Entropy Alloys

Beiya Wang ¹, Chao Yang ^{1,*}, Da Shu ^{1,2,*} and Baode Sun ^{1,2}¹ Shanghai Key Lab of Advanced High-Temperature Materials and Precision Forming, School of Materials Science and Engineering, Shanghai Jiao Tong University, Shanghai 200240, China; bdsun@sjtu.edu.cn (B.S.)² State Key Lab of Metal Matrix Composites, School of Materials Science and Engineering, Shanghai Jiao Tong University, Shanghai 200240, China

* Correspondence: yangchao1987@sjtu.edu.cn (C.Y.); dshu@sjtu.edu.cn (D.S.)

Abstract: Along with the globalization of environmental problems and the rapid development of the field of nuclear technologies, the severe irradiation damage of materials has become a big issue, restricting the development of advanced nuclear reactor systems. Refractory high-entropy alloys (RHEAs) have the characteristics of a complex composition, a short-range order, and lattice distortion and possess a high phase stability, outstanding mechanical properties, and excellent irradiation resistance at elevated temperatures; thus, they are expected to be promising candidates for advanced nuclear reactors. This review summarizes the design, preparation, and irradiation resistance of irradiation-tolerant RHEAs. It encompasses a comprehensive analysis of various aspects, including the evolution of defects, changes in microstructure, and the degradation in properties. Furthermore, the challenges and insufficiently researched areas regarding these alloys are identified and discussed. Building on this foundation, the review also provides a forward-looking perspective, outlining potential avenues for future research.

Keywords: refractory high-entropy alloys; irradiation damage; nuclear power



Citation: Wang, B.; Yang, C.; Shu, D.; Sun, B. A Review of Irradiation-Tolerant Refractory High-Entropy Alloys. *Metals* **2024**, *14*, 45. <https://doi.org/10.3390/met14010045>

Academic Editors: Martin Heilmair and Seok Su Sohn

Received: 5 December 2023

Revised: 27 December 2023

Accepted: 27 December 2023

Published: 29 December 2023



Copyright: © 2023 by the authors. Licensee MDPI, Basel, Switzerland. This article is an open access article distributed under the terms and conditions of the Creative Commons Attribution (CC BY) license (<https://creativecommons.org/licenses/by/4.0/>).

1. Introduction

The environmental problems caused by traditional fossil fuels are increasingly prominent, and the development and utilization of clean energy have become a global issue. Nuclear energy has many advantages, such as a high energy density, great power generation efficiency, low comprehensive cost, continuous power supply, and small regional climate impact, but the inherent safety of nuclear reactors is a key issue limiting its development [1]. The properties of structural/cladding materials are fundamental in the inherent safety; however, they are affected by long-term irradiation of high-temperature and high-energy neutrons and fission products, which usually causes thermal stress expansion and cracks, in addition to radiation hardening and embrittlement [2–5], radiation swelling [6], phase transformations [7,8], helium effect behavior [9], etc.

Due to the exposure of materials to high-energy radiation, changes at the atomic level in the materials cause embrittlement. For instance, radiation-induced changes in the crystal structure create additional obstacles to dislocation movement, making the material more brittle. They may also lead to the nucleation and growth of precipitate phases within the material, which serve as initiation points for cracks and significantly affect the ductility and strength of the material. Elements like helium, produced by radiation reactions, tend to accumulate preferentially at these grain boundaries, leading to intergranular cracking and thereby increasing the brittleness of the material. Helium also forms bubbles within the lattice, causing swelling and further embrittlement. Temperature has a significant impact on materials as well. At lower temperatures, defect mobility is restricted, resulting in higher concentrations of point defects and dislocation loops. As the temperature increases, some defects may annihilate each other. However, higher temperatures can also accelerate diffusion-driven processes, which can lead to precipitation and grain boundary segregation.

In the past 70 years, many researchers have thrown themselves into nuclear structural/cladding material research and developed several alloy systems. Aluminum alloy [10] was used only at low operating temperatures (below 150 °C) in the early stages of nuclear reactor development due to its low neutron absorption cross-section, and it was gradually replaced by other alloys as the temperature and power of reactors increased. Nickel-based superalloys [11–13] and zirconium alloys [14,15] can work at temperatures above 400 °C, but they have a big problem of hydrogen absorption. For instance, due to the high temperature, high pressure, and strong oxidation and corrosivity, the material in a supercritical water-cooled reactor suffers hydrogen embrittlement, which makes the material fail quickly. In order to solve the problem of hydrogen absorption of the material, nickel is no longer added into the Zr-4 alloy; however, the radiation-induced swelling of this alloy is much higher. Austenitic stainless steel is used in some fast and gas-cooled reactors. Although austenitic stainless steel (FCC) has a low thermal conductivity and its swelling resistance [16] and yield strength need to be improved. Ferritic/martensitic steel (RAFM) with a BCC structure has good swelling resistance; however, the high-temperature irradiation environment instability leads to a sharp decline in mechanical properties due to the negative effect of impurities in RAFM [17]. ODS steel possesses a high irradiation resistance and good mechanical properties; nevertheless, its highly difficult preparation and processing and poor long-term phase stability under severe operating conditions limit its application potential [18,19]. Due to the relatively moderate operating environment of Generation I to III nuclear reactors, these traditional nuclear materials meet the existing requirements, although they are not perfect.

The concept of Generation IV nuclear reactors was proposed to improve the inherent safety of nuclear systems in 2002 [20]. They possess the characteristics of miniaturization and modularization and have great application potential in extreme environments such as aerospace, islets, deserts, plateaus, polar regions, and deep seas, which leads to the prospect of dual use in military and civilian applications. With the development of Generation IV nuclear reactors, stricter requirements have been established to ensure their safe operation and the continuous supply of energy. However, their harsh coupling operating conditions, including elevated temperatures, substantial radiation damage, and high He concentrations [21], present severe challenges for their materials [22]. Although conventional alloys have developed rapidly in the past few decades, their properties are far from satisfactory. Thus, research on novel materials with superior comprehensive properties is in huge demand and has high prospects [7].

High-entropy alloys (HEAs) have attracted increasing attention [23] due to their high entropy effect, lattice distortion effect, sluggish diffusion, and cocktail effect [24]. These effects make it difficult for HEAs to accumulate defects in irradiation environments and provide new possibilities for advanced nuclear reactors. Radiation-tolerant 3D transition group HEA systems with a face-centered cubic (FCC) structure have been widely studied in recent years. To compare the effects of different elements and components on the irradiation performance, Lu and Jin et al. [25] started their research on pure Ni in an FCC system and gradually added components from binary NiCo and NiFe. Later three- to five-element alloys include CoCrNi [26], FeCoNi, CoCrFeNi [27], FeMnCoNi, and CoCrFeMnNi [28]. As the composition complexity of the alloy increases, it is found that its irradiation resistance also improves because the high entropy leads to a change in the interstitial atom–vacancy migration energy barrier, resulting in less lattice damage. In particular, the five-element alloy NiCoFeCrMn has excellent mechanical properties and its swelling resistance is 40 times higher than nickel, but it might not be ideal for nuclear applications due to the presence of Co, which can become radioactive ^{60}Co upon neutron absorption. Wang et al. [29] compared the approximate component alloys (Ni, NiFe, NiCo, NiFeCr, NiFeCo) and found that with the increase in the number of elements from one to three, the size of helium bubbles tended to decrease, except for Cr ternary alloys. It was found that Cr can exchange with vacancies to cause vacancy accumulation and promote the growth of helium bubbles. However, research on helium embrittlement and the swelling

resistance of FCC alloys containing nickel shows the opposite, because Ni has a high neutron activation and an adverse effect on the hydrogen absorption of materials, which make the alloy susceptible to transmutation under irradiation. To sum up, it was found in previous studies that many elements in the 3D transition group possess high neutron absorption and activation, which are not ideal for nuclear applications. In addition, HEAs with a body-centered cubic (BCC) structure have begun to be explored owing to their higher resistance to helium embrittlement and swelling [5,12,30,31]. Therefore, new HEA systems with a BCC structure have recently attracted attention.

As one type of HEA, refractory high-entropy alloys (RHEAs) are mainly composed of multiple principal refractory elements [7,8,30]. They possess a BCC structure, good phase stability, and high melting points and operating temperatures, and have good prospects in nuclear applications. However, research on RHEAs in the nuclear field has just started and they have not been systematically studied yet. A lot of studies are required before RHEAs can be used in advanced nuclear reactor systems. This review aims to provide assistance for in-depth research of radiation-tolerant RHEAs in future by summarizing and organizing the current research on RHEAs.

2. Composition Design and Preparation of RHEAs

The composition of RHEAs is notably diverse, which consequently imparts a variety of effects on material properties. This diversity adds complexity to material design, as selecting suitable ratios and combinations from myriad possibilities is a key focus in current alloy design. Two primary challenges arise in the design of these alloys: the selection of proper elements and the appropriate proportions of these elements. Leveraging the cocktail effect, one of the four core effects of HEAs, certain elements can be chosen based on their intrinsic properties to achieve specific performance goals. For instance, Ti can be selected to reduce density and enhance ductility [32,33], Cr can be selected for its oxidation resistance [34–36], and Zr can be selected for its low thermal neutron absorption cross-section [37–39].

In terms of designing RHEAs with a high radiation resistance, neutron absorption and activation should be considered as a priority from the outset. A low neutron absorption cross-section is a crucial requirement for radiation-resistant alloys, as it enhances the neutron economy of nuclear reactors. Table 1 summarizes refractory elements and those with low neutron absorption cross-sections. It is observed that, with the exception of Hf, which has a thermal neutron absorption cross-section of 104.1 barns [40], most refractory elements have relatively low neutron absorption cross-sections. Notably, Zr has a neutron absorption cross-section of only 0.186 barns [37], making it particularly well suited for use in nuclear reactors.

Following the selection of elements for RHEAs, it becomes imperative to determine the proportion of each element. This determination can be guided by empirical methods, computational simulations, or high-throughput experimental approaches. Thermodynamic considerations such as configurational entropy, mixing enthalpy, melting point, atomic size difference, and valence electron concentration offer a framework to establish a reasonable range for these proportions. The use of phase diagram calculations further elucidates the impact of temperature on phase composition, facilitating the assessment of alloy phase stability. Additionally, employing first principles calculations [41,42] from a thermodynamic perspective enables a deeper analysis of the alloy. This approach yields critical data, including entropy, enthalpy, and Gibbs free energy, which are essential for comprehending the thermodynamic properties and potential performance of the alloy. Such a comprehensive analysis is integral to optimizing the design of HEAs for specific applications, particularly in demanding environments where material stability and performance are crucial.

The fabrication of RHEAs can be accomplished through various advanced techniques, such as magnetron sputtering [8,43] and laser metal deposition (LMD) [44,45]. However, to produce bulk materials, vacuum arc melting [46] is the most prevalent method. This technique is widely favored due to its efficiency in producing high-quality, homogeneous

alloys. A smaller proportion of RHEA production utilizes alternative methods like levitation melting [47] and powder metallurgy [48]. While a variety of techniques is available for the preparation of RHEAs, the choice of method largely depends on the specific requirements of the alloy being produced, including its composition, desired properties, and intended application.

Table 1. Fundamental information on refractory elements and select elements that form secondary phases [40,49,50].

Symbol	Name	Atomic Number	Atomic Weight	Type	Ionization Energy (eV)	Melting Point (°C)	Boiling Point (°C)	Crystal Structure	Atomic Radius (Display)	Metallic Radius (pm)	Covalent Radius (pm)	Density (g/cm³)
B	Boron	5	10.811	Metalloids	8.298	2075	4000	rhom.	(v) 82	-	82	2.46
C	Carbon	6	12.011	Non Metal	11.260	3550	4027	hex	(v) 77	-	77	2.26
Al	Aluminum	13	26.982	Poor Metal	5.986	660.32	2519	FCC	(m) 143	143	118	2.70
Si	Silicon	14	28.086	Metalloids	8.152	1414	2900	cubic	(v) 111	-	111	2.33
Ti	Titanium	22	47.867	Transition Metal	6.828	1668	3287	HCP	(m) 147	147	136	4.51
V	Vanadium	23	50.942	Transition Metal	6.746	1910	3407	BCC	(m) 134	134	125	6.11
Cr	Chromium	24	51.996	Transition Metal	6.767	1907	2671	BCC	(m) 128	128	127	7.14
Zr	Zirconium	40	91.224	Transition Metal	6.634	1855	4409	HCP	(m) 160	160	148	6.51
Nb	Niobium	41	92.906	Transition Metal	6.759	2477	4744	BCC	(m) 146	146	137	8.57
Mo	Molybdenum	42	95.940	Transition Metal	7.092	2623	4639	BCC	(m) 139	139	145	10.28
Hf	Hafnium	72	178.490	Transition Metal	6.825	2233	4603	HCP	(m) 159	159	150	13.31
Ta	Tantalum	73	180.948	Transition Metal	7.550	3017	5458	BCC	(m) 146	146	138	16.65
W	Tungsten	74	183.840	Transition Metal	7.864	3422	5555	BCC	(m) 139	139	146	19.25

Symbol	Atomic Radius (calculated) (pm)	Electro-negativity (Pauling)	Elasticity (Gpa)	Thermal neutron absorption cross-section (barns)	Thermal Conductivity, W/(m K)	Latent Heat of Fusion (kJ/mol)	Yield strength (MPa)	UTS (Mpa)	Van der Waals Radius, (pm)	Hardness (HV)	Electrical Resistivity (Ωm)	Electron Affinity (kJ/mol)
B	87	2.04	-	760.30	27	50.2	-	-	192	4998	1.0×10^4	26.7
C	67	2.55	-	0.0035	140	-	-	-	170	-	1.0×10^{-5}	153.9
Al	118	1.61	69	0.23	235	10.79	15	90	184	17.034	2.6×10^{-8}	42.5
Si	111	1.90	150	0.171	150	50.55	165	170	210	-	1.0×10^{-3}	133.6
Ti	176	1.54	116	6.096	22	15.45	450	520	-	81.6–346.8	4.0×10^{-7}	7.6
V	171	1.63	128	5.086	31	20.9	770	800	-	64.26	2.0×10^{-7}	50.6
Cr	166	1.66	279	3.05	94	16.9	131	550	-	105.06	1.3×10^{-7}	64.3
Zr	206	1.33	88	0.186	23	16.9	230	330	-	91.8	4.2×10^{-7}	41.1
Nb	198	1.60	105	1.156	54	26.4	70	275	-	132.6	1.5×10^{-7}	86.1
Mo	190	2.16	330	2.60	139	32	-	324	-	156.06	5.0×10^{-8}	71.9
Hf	208	1.30	78	104.1	23	24.06	125	480	-	173.4	3.0×10^{-7}	0
Ta	200	1.50	186	20.5	57	31.6	705	760	-	88.74	1.3×10^{-7}	31
W	193	2.36	750	18.3	170	35.4	411	980	-	357	5.0×10^{-8}	78.6

3. Irradiation Resistance of RHEAs

The degradation of the macroscopic properties of alloys caused by radiation damage is one of the most important reasons for the failure of materials in reactors. High-energy particles such as neutrons, electrons, protons, and ions interact with the alloy, resulting in point defects such as vacancies and atom gaps, which gradually evolve into changes in microstructure and finally lead to a degradation in material properties. At present, the most studied radiation damage includes irradiation hardening, embrittlement, swelling, phase transitions, and high-temperature helium and hydrogen embrittlement. Some researchers have studied the radiation damage of RHEAs.

3.1. Irradiation Hardening and Embrittlement

In nuclear applications, materials are often exposed to extreme radiation, which can lead to irradiation hardening: an increase in material hardness and brittleness due to the formation of defects like dislocation loops and voids in the crystal lattice. This phenomenon can severely impact the performance and safety of nuclear reactors [51]. Kumar et al. [52] conducted a study on the variations in the mechanical properties and microstructure of RHEAs after irradiation. The hardening mechanism model is depicted in Figure 1 [5]. They discovered that RHEAs have commendable resistance to radiation hardening and maintain stability following ion irradiation.

Kareer et al. conducted ion irradiation experiments using 2 MeV V⁺ ions on four different alloys at 500 °C, with an irradiation fluence of 2.26×10^{15} ions/cm². Observations were made on pure V and the high-entropy alloys TiVNbTa, TiVZrTa, and TiVCrTa. It was found that pure V exhibits the most significant change in hardness, approximately 37%, prior to and following irradiation. In contrast, the three RHEAs showed relatively minor changes in hardness, with TiVNbTa exhibiting a hardening rate of about 6%. No-

tabley, the low-activation TiVZrTa and TiVCrTa RHEAs demonstrated negligible hardening rates, as shown in Figure 2a. Correlating with the neutron absorption cross-section data provided in the accompanying Table 1, Zr indeed has the smallest cross-section, indicating a higher resistance to irradiation [53]. At the University of North Texas [4], in an irradiation experiment with 4.4 MeV high-energy Ni^{2+} ions at a fluence of 1.08×10^{17} ions/cm² at room temperature, the radiation response of HfTaTiVZr RHEAs was compared to that of conventional 304 stainless steel. It was observed that HfTaTiVZr RHEAs undergo a modest increase in hardness and yield strength by about 13% and 28%, respectively; a contrast to the significant increases in 304 stainless steel, which exhibits 50% and 54% enhancements in these mechanical properties (Figure 2b). This disparity is attributed to the inherently sluggish diffusion of atoms in RHEAs, which impedes the mobility of interstitials, resulting in a superior irradiation resistance. Such findings underscore the potential of HfTaTiVZr RHEAs as more resilient materials subject to high radiation exposure.

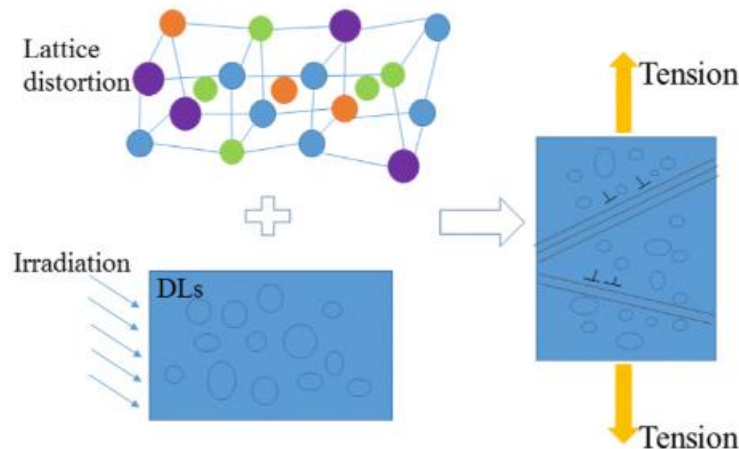


Figure 1. A model of the hardening mechanism. The severe lattice distortion, dislocation and irradiation-induced dislocation loops are considered in the model of RHEAs. (Reprinted with permission from ref. [5]. Copyright 2021 Elsevier.)

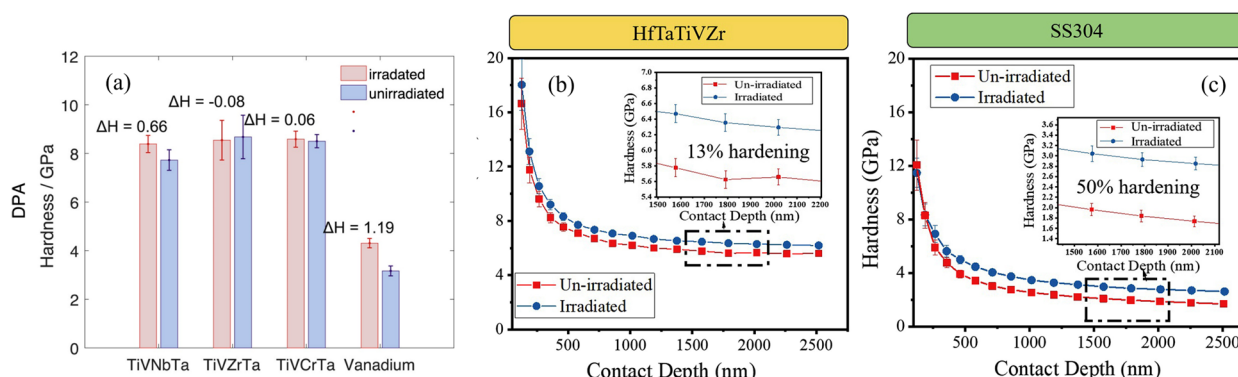


Figure 2. (a) Indentation hardness of irradiated and unirradiated HEAs and control sample at 300 nm indentation depth [53]. Hardness versus depth for irradiated and un-irradiated samples of (b) HfTaTiVZr HEA and (c) 304 stainless steel [4]. (Reprinted with permission from refs. [4,53]. Copyright 2019 and 2020 Elsevier.)

Chang et al. [31] explored the irradiation resistance of the HfNbTaTiZr RHEAs. The experiment involved subjecting samples of the HfNbTaTiZr alloy to 300 keV Ni^{+} ion bombardment at a fluence of 1.5×10^{16} cm⁻² at 100 °C, with a damage level of over 30 dpa. The researchers discovered that irradiation-induced swelling is remarkably suppressed in the HfNbTaTiZr alloy. The nanoindentation hardness after irradiation is almost unchanged, indicating a high resistance to hardening due to irradiation. This suggests that the material

experiences extensive lattice distortion and has altered diffusion kinetics under irradiation. The lattice distortion and diffusion kinetics of RHEAs like HfNbTaTiZr endow them with superior radiation tolerance. The results reveal that the swelling and hardening effects in HfNbTaTiZr RHEAs are significantly suppressed compared to those in conventional nuclear materials.

Moschetti et al. [54,55] investigated the room-temperature mechanical behavior of TiZrNbHfTa RHEAs after ion irradiation, revealing their resistance to He irradiation damage. It was found that the strength and ductility of the TiZrNbHfTa RHEAs are well maintained after irradiation. The results of the study indicate that TiZrNbHfTa RHEAs exhibit only a 13.9% increase in hardness (hardening), while a 4.5% of increase in elongation, suggesting a high resistance to He-induced hardening and embrittlement (Figure 3). Nanoscale He bubbles were found within the grain boundaries, as shown in Figure 3. The authors believe that these bubbles are contributing factors in the activation of a grain boundary gliding mechanism, which helps the material to maintain a certain ductility. The presence of helium bubbles weakens the grain boundaries of the alloy, allowing for movement or sliding at the grain boundaries under stress.

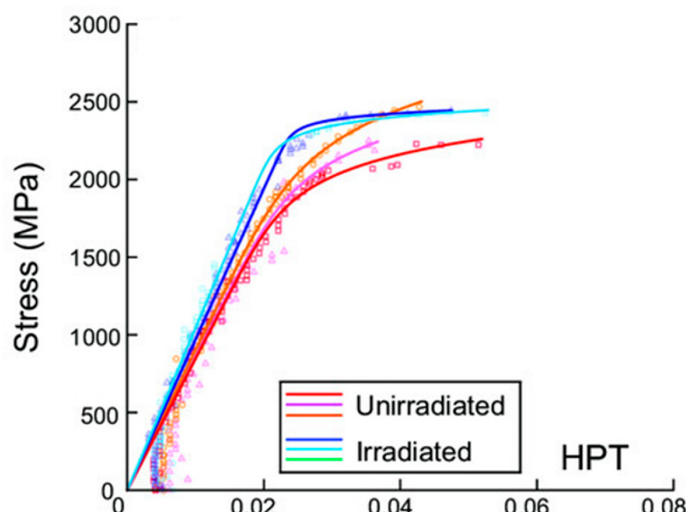


Figure 3. Tensile stress–strain curves of both irradiated and unirradiated HPT [55]. (Reprinted with permission from ref. [55]. Copyright 2023 John Wiley and Sons.)

El Atwani et al. [43] focus on nanocrystalline RHEAs composed of W, Ta, Cr, V, and Hf. This composition was determined through techniques like thermophysical parameter calculations and the Calculation of Phase Diagrams (CALPHAD) method. Quinary RHEAs exhibit microstructural stability and a promising ion irradiation response under single- and dual-beam ion irradiation conditions, attributed to factors like the high density of stable grain boundaries, the chemical complexity affecting defect recombination rates, and a lower order-disorder transition temperature compared to the original four-element RHEAs. Dislocation loops are not detected even after significant helium implantation and irradiation. A study of cavity density and size shows no increasing trends in these parameters, indicating a saturation effect under the tested irradiation conditions. Furthermore, nanoindentation tests conducted before and after annealing and irradiation reveal changes in the hardness of the alloy. The substantial hardening of the alloy under irradiation conditions reaches 20 GPa (unirradiated sample: 13.25 GPa and annealed sample: 16.25 GPa). The microstructure and irradiation-induced hardening of a group of BCC-structured alloys (MoNbTaTi, MoNbTa, and MNbTaTiW) were observed via the CALPHAD method at Hokkaido University, Japan [56]. It was found that MoNbTa-based BCC RHEAs have quite a good high-temperature stability, and it is speculated that due to the high entropy of HEAs, the radiation hardening of MoNbTaTiW is smaller than that of MoNbTaTi. The radiation hardening of both alloys is smaller than that of pure W.

3.2. Irradiation-Induced Phase Transformations of RHEAs

The phenomenon of the segregation of alloy elements caused by irradiation was firstly postulated by L.E. Anthony in 1972 [57]. At Argonne National Laboratory, the segregation effects of principal and trace elements within the matrix of both binary and ternary alloy systems were studied using techniques like Auger electron spectroscopy to reveal the complex changes in materials exposed to radiation [58]. It was found that the segregation of elements can affect the mechanical properties of materials. Under irradiation, the movement of vacancies and interstitial atoms in the material promotes diffusion, leading to element segregation and precipitation, resulting in enrichment and depletion of elements. The movement of point defects promotes the movement of solute atoms. When the radius of body atoms is larger than that of solute atoms, solute are easily combine with collective atoms to form a positive binding energy; these atoms move to defect traps such as grain boundaries, so solute atoms precipitate at the grain boundaries under irradiation conditions. On the contrary, when the radius of the matrix atom is smaller than that of the solute atom, the solute atom easily combines with the collective atom to form a negative binding energy. The atoms move away from the boundary, so the phenomenon of solute atom dilution occurs at the grain boundary.

Pu et al. [8] discuss the mechanisms of irradiation-induced crystallization in amorphous TaTiWVCr RHEAs and W films when exposed to 60 keV He⁺ ion irradiation. Both materials were irradiated using a 60 keV He ion beam platform, with fluences ranging from $1 \times 10^{16} \text{ cm}^{-2}$ to $2 \times 10^{17} \text{ cm}^{-2}$. Defect accumulation increases the free energy and triggers crystallization when a critical concentration is reached. This process is propelled by the thermal-spike effect, where energy transfer from hot electrons to the cooler lattice causes short-range diffusion and a rise in the lattice temperature. Grain growth is further aided by interactions at the grain boundaries (GBs) between amorphous and nano-crystalline areas, reducing the GB's curvature. He⁺ ion irradiation introduces vacancies and interstitial defects, enhancing atomic mobility and rearrangement and thus forming nanometer-sized grains. Additionally, irradiation causes compositional reorganization in the RHEAs, where metallic atoms diffuse and become entrapped by GBs, facilitating grain growth. Theoretical simulations show that the amorphous–crystalline boundary advances into the amorphous zone over time, Figure 4, forming spherical or ellipsoidal grains through atomic entrapment. Continuous ion irradiation at a high fluence results in fast grain growth, induced by a disorder-driven mechanism that promotes preferential growth in grains with a {110} direction on a much shorter timescale than curvature-driven or grain-rotation mechanisms. Tunes et al. [59] observed the changes in the chemical composition of two RHEAs before and after irradiation. They found that the crystalline region of the WTaCrV alloy shows no significant changes before and after irradiation, while small Hf-rich precipitates are observed in WTaCrVHf after irradiation at 800 °C.

The NbZrTi series of RHEAs has excellent phase stability and high mechanical properties at elevated temperatures [60], such as NbZrTiHf [61,62], NbZrTiTaHf [31,63,64], NbZrTiV [65], NbZrTiMoV [66], etc. Their lattice distortion and composition complexity have obvious inhibition effects on heavy ion irradiation [67]. Lei et al. [68] focused on improving the damping properties of Ta0.5Nb0.5HfZrTi by doping with oxygen or nitrogen. These enhanced materials show promise in eliminating noise and mechanical vibrations, crucial for various applications. This research indicates that these doped RHEAs exhibit not only good damping properties but also an improved strength and ductility. They are promising as a cladding material for high-power nuclear reactor systems. A team from Xi'an Jiao Tong University [7] analyzed the point defect properties of NbZrTi RHEAs using first principles calculations. They found that severe lattice distortion in these alloys leads to instability in conventional vacancies and interstitial structures. This results in a lower average formation energy for vacancies and interstitials compared to pure Nb. They also observed a wide distribution of vacancy migration energies and slow interstitial diffusion (Figure 5). Additionally, Ti atoms show fast diffusion rates under irradiation. NbZrTi shows reduced void formation at high temperatures due to its altered vacancy and interstitial

behaviors. There is a wide range of vacancy migration energies, extending to 0 eV, leading to preferential migration through low barrier sites. Interstitial diffusion is slower than that in pure Nb, mainly due to reduced long $\langle 111 \rangle$ diffusion pathways caused by variations in stable interstitial orientations.

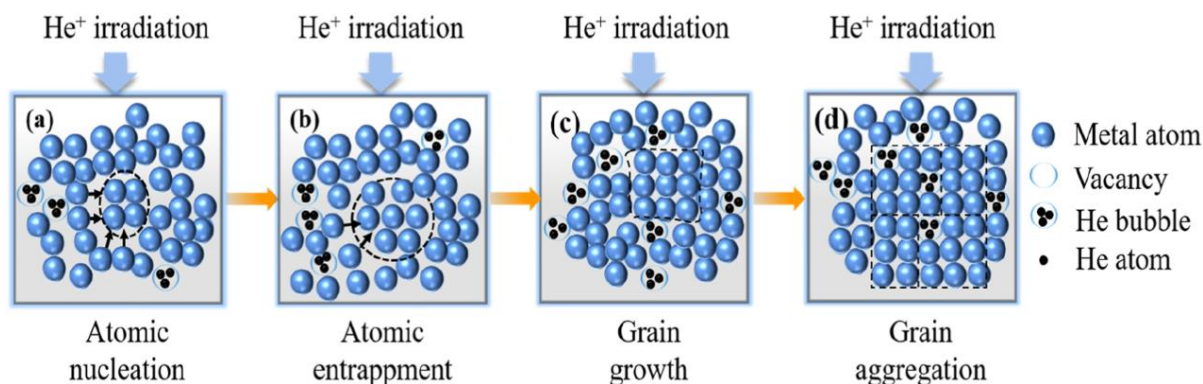


Figure 4. Illustration of irradiation-induced grain growth in TaTiWVCr or W films constructed with amorphous structures. (a) atomic nucleation, (b) atomic entrapment, (c) grain growth and (d) grain aggregation (Reprinted with permission from ref. [8]. Copyright 2023 Elsevier.)

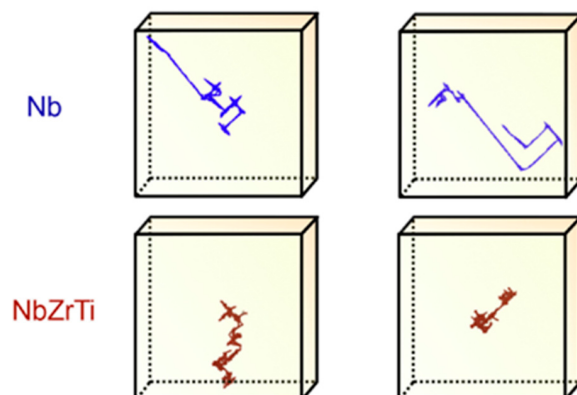


Figure 5. Representative trajectories of interstitial pairs in NbZrTi and Nb with the same diffusion time scale. The interstitial trajectories are unwrapped from the simulation box with periodic boundaries and are enclosed here in boxes of the same length scale. (Reprinted with permission from ref. [7]. Copyright 2022 Elsevier.)

The irradiation of RHEAs is studied by a combination of simulations and experiments. Egami et al. [69] report that due to local melting caused by thermal spikes and recrystallisation caused by different atomic sizes, high atomic-level stresses in ZrHfNb can promote the amorphous phase via irradiation and lead to much less defects. They reveal that ZrHfNb has less defects and a good resistance to electron damage via simulations of the kinetic damage of displacing atoms and molecular dynamics simulations of the thermal spike of energy deposition.

3.3. Irradiation Effect of Helium

The nuclear reaction between neutrons and materials can produce hydrogen and helium, and the helium generated by transmutation is not easily diffused in the material because of its low solubility. Hydrogen is easily diffused out of the material under high-temperature conditions; hydrogen and helium in the alloy further accelerate the diffusion of atoms in the material under irradiation with the capture and diffusion among crystal defects, such as vacancy point defects, dislocation rings, and interstitial atomic clusters. This results in phase precipitation and element segregation in the material, making the material

undergo hydrogen embrittlement or helium embrittlement [70]. The formation of defect groups through the combination and decomposition of defects leads to radiation swelling of the material. Defects such as dislocation rings lead to hardening of the material. When the irradiation temperature is greater than 0.5 Tm, helium ions generated by transmutation reactions in the nuclear material form helium bubbles or cavities under the action of stress, which causes swelling inside the material, resulting in further improvements in the brittleness of the material [71]. High-temperature helium embrittlement can be used as one of the reference standards to determine the highest temperature of structural materials in a neutron irradiation environment.

Jia et al. [72] compared three different single-phase BCC structure alloys, V-alloy, TiVTa and TiVNbTa alloys, after irradiation by He ions (1.5 MeV) at fluences of 2×10^{16} and 1×10^{17} ion/cm² at 700 °C. By comparing the width of the He bubble formation region in Figure 6a–c under 1×10^{17} ion/cm², it was found that V-alloy has the narrowest region, indicating that helium diffuses the slowest in V-alloy, while the wider distribution of He bubbles in TiVTa and TiVNbTa suggests that helium diffuses relatively fast in these two alloys. Especially for TiVTa, they observed He bubble clusters in the irradiation peak region. They found that the density and size of He bubbles in these three alloys increase with the increase in fluence, which is the same trend as the simulation results. The yellow arrow in Figure 6d,e shows that V accumulates around He bubbles and Ti, Nb, and Ta are depleted around the He bubbles.

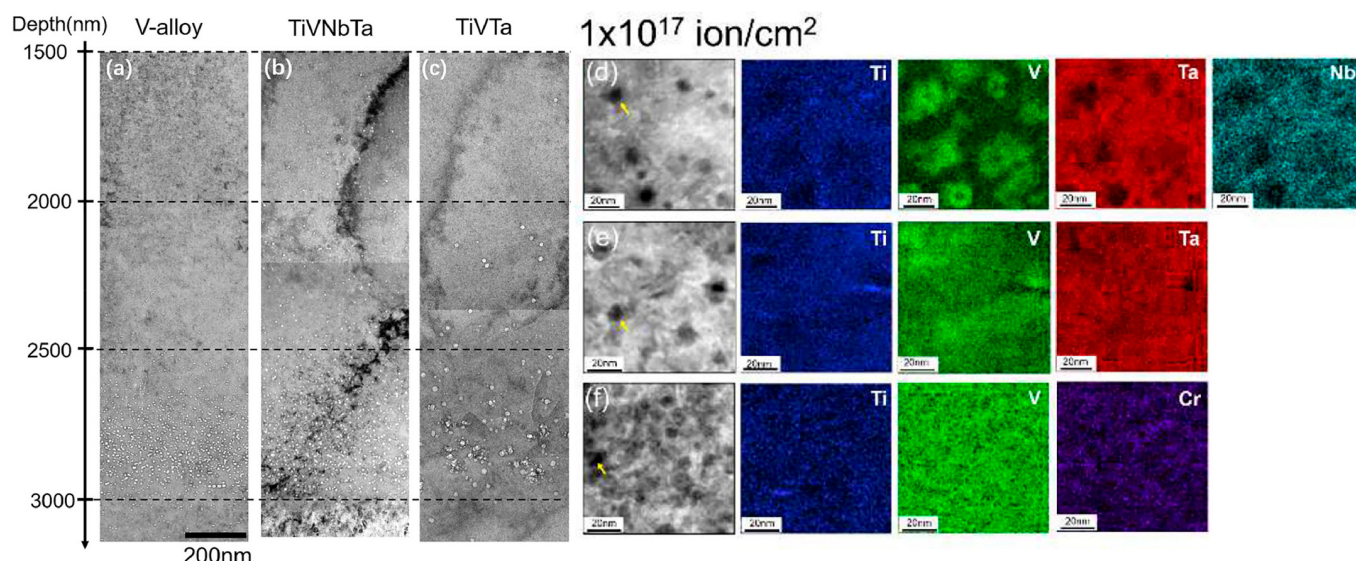


Figure 6. Under-focused TEM-BF images showing the He bubble distribution under a fluence of 1×10^{17} ion/cm² in (a) V-alloy, (b) TiVNbTa, and (c) TiVTa between 1500 and 3200 nm below the surface. STEM-HAADF images and the corresponding EDS mappings of the He bubbles in the peak region of the samples irradiated with a fluence of 1×10^{17} ion/cm², showing the elemental distribution around the He bubbles. (d) TiVNbTa, (e) TiVTa, (f) V-alloy. (Reprinted with permission from ref. [72]. Copyright 2021 Elsevier.)

Cui et al. [30] studied the irradiation behaviors of pure W and W-rich RHEAs (RHEA-W). The RHEA-W alloys consist of ultrafine grains with a body-centered cubic (BCC) structure. They are composed of W-based and Ti-rich grains with an ultrafine grain size, which is significantly finer than that of pure W. These alloys exhibit excellent surface stability under He irradiation. With an irradiation fluence of 0.9×10^{25} ions/m², the surface of the RHEA-W alloys remains nearly flat. The impressive stability of these alloys under He⁺ irradiation is attributed to their self-healing mechanism. The high-entropy matrix undergoes microstructural rearrangement to fill in damaged areas, atom diffusion to repair defects, phase transformations that mitigate damage, and potential chemical reactions.

Guo et al. [73] and Senkov et al. [74] studied nanocrystal NbMoTaW and NbMoTaWV RHEA films under high-dose and low-energy helium ion irradiation at 777 °C. It was found that the alloys maintain a BCC structure, and neither the thermal conductivity nor the electrical conductivity decreases. This indicates that the alloys can inhibit the diffusion of helium and effectively inhibit the growth of helium bubbles after the introduction of V (Figure 7a,b). The accumulation and clustering of helium bubbles may be mitigated by adjusting the formation and migration energies of helium and vacancies, thereby enhancing the ability of the material to accommodate helium. The introduction of V further enhances the lattice distortion of the alloy, indicating that the lattice distortion greatly inhibits the diffusion of helium ions. By measuring the resistivity and conductivity of two alloy films before and after irradiation, it is observed that with the increase in fluence, the resistivity of the alloy films progressively decreases, while their conductivity gradually increases. The increase in fluence leads to the coalescence of small grains into larger grains, significantly reducing electron scattering caused by grain boundaries. This results in a decrease in the overall resistivity of the films. Moreover, defects such as helium bubbles in the irradiated films contribute to an increase in electron scattering, thereby elevating the resistivity (Figure 7c,d).

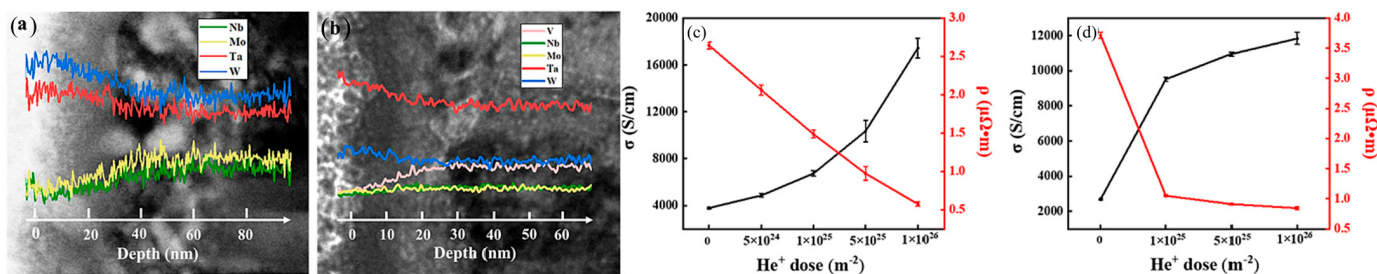


Figure 7. Cross-sectional TEM images and corresponding line scan energy spectra of (a) a NbMoTaW RHEA film and (b) a NbMoTaWV RHEA film after irradiation with He⁺ at an irradiation fluence of 1.0×10^{26} ions/m². The resistivity and conductivity variations curves of (c) NbMoTaW RMPEA films and (d) NbMoTaWV RHEA films before and after different fluences of He⁺ irradiation. (Reprinted with permission from ref. [73]. Copyright 2022 Elsevier.)

The alloys compositions of MoNbTiVCr and MoNbTiVZr RHEAs have a low thermal neutron absorption cross-section and a high thermal conductivity [38]. They have superior irradiation resistance and high-temperature corrosion resistance. Through an experiment of He ion simulations of neutron irradiation, it was found that Mo_{0.5}NbTiVCr_{0.25} is stable at lower irradiation levels but shows signs of amorphization at higher fluences. Moreover, both alloys exhibit slight irradiation hardening. Dislocation loops are formed in BCC-structure HEAs after irradiation. The dislocation loops are similar in size (4–6 nm) but vary in density (Figure 8). After exposure to high doses of irradiation, it is observed that there is a notable increase in the number of dislocation loops, while the size of these loops remains unchanged. This phenomenon can be attributed to the significant lattice distortion present in RHEAs. The lattice distortion in these alloys creates barriers to the migration of point defects, effectively controlling the growth of dislocation loops. The presence of lattice distortion is a hallmark characteristic of RHEAs, resulting from their complex multi-element composition. This distortion leads to an irregular lattice structure, which hinders the movement of atoms and defects within the material. Due to lattice distortion and composition complexity, the material reaches the irradiation damage peak late, and no sediment is found after irradiation. This indicates that this material is one of the candidates for fuel cladding materials with good accident resistance [75]. The chemical long-range disorder of RHEAs increases the scattering of electrons and results in a slowdown in the energy consumption of the cascade collision, thus prolonging the thermal peak time and increasing the probability of defect recovery.

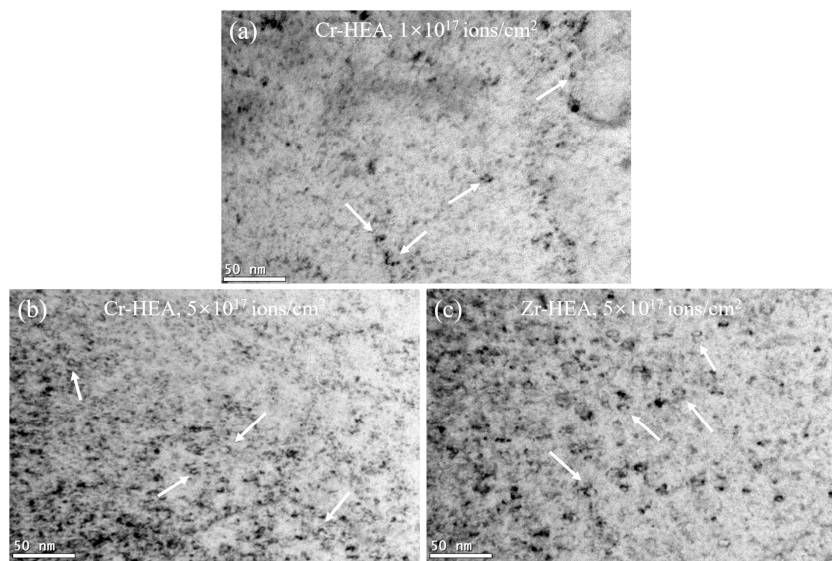


Figure 8. Cross-section TEM BF images of the specimens irradiated by helium ions: (a) a Cr-HEA at ion fluences of 1×10^{17} ions/cm 2 , (b) a Cr-HEA at ion fluences of 5×10^{17} ions/cm 2 , (c) a Zr-HEA at ion fluences of 5×10^{17} ions/cm 2 . Some irradiation-induced dislocation loops are marked by white arrows. (Reprinted with permission from ref. [75]. Copyright 2021 Elsevier.)

Lu et al. [76] found that $\text{Ti}_2\text{ZrHfV}_{0.5}\text{Mo}_{0.2}$ RHEAs have an exceptional irradiation resistance and exhibit minimal hardening and a unique reduction in the lattice constant upon exposure to He-ion irradiation. In conventional alloys, X-ray diffraction (XRD) peaks typically shift to the left with an increase in the lattice constant following irradiation. However, in the case of the $\text{Ti}_2\text{ZrHfV}_{0.5}\text{Mo}_{0.2}$ HEA, the opposite trend is observed, where the XRD peaks move to the right, accompanied by a decrease in the lattice constant after irradiation, as shown in Figure 9a. The high concentration of vacancy defects in the alloy plays a role in trapping He atoms. This mechanism significantly reduces the formation of helium bubbles along grain boundaries, thereby mitigating the brittleness typically induced by irradiation in RHEAs (Figure 9b). Additionally, the limited formation of helium bubbles within the matrix contributes to a substantial decrease in irradiation hardening of the alloy. This characteristic of this HEA is attributed to its high-density lattice vacancies/defects, which confer exceptional irradiation tolerance.

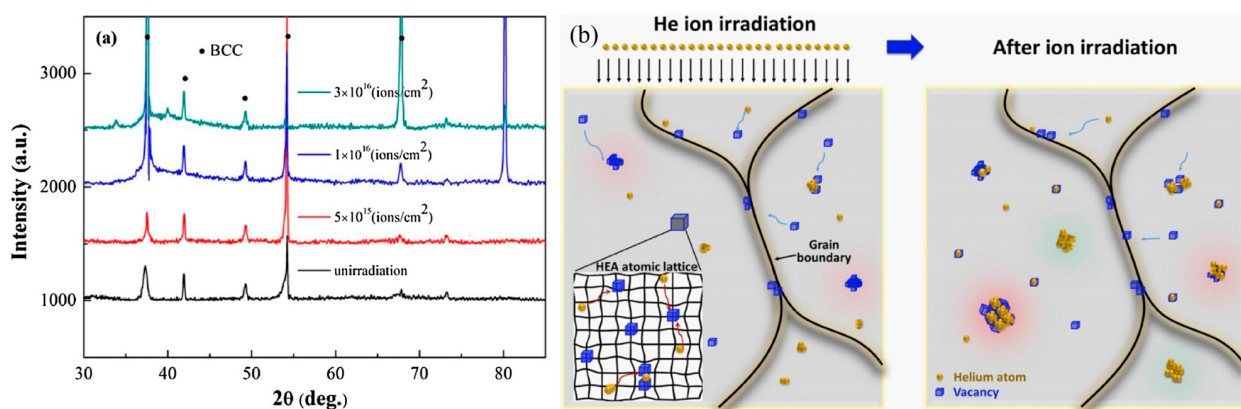


Figure 9. (a) XRD patterns of initial and irradiated $\text{Ti}_2\text{ZrHfV}_{0.5}\text{Mo}_{0.2}$ HEA at ion doses of 5×10^{15} , 1×10^{16} , and 3×10^{16} ions/cm 2 , respectively. (b) A schematic diagram of He ions being captured in the vacancy defects of the $\text{Ti}_2\text{ZrHfV}_{0.5}\text{Mo}_{0.2}$ HEA. (Reprinted with permission from ref. [76]. Copyright 2018 Elsevier).

4. Summary

The introduction of refractory elements into BCC-structured HEAs can further improve their high-temperature mechanical properties. Although stable BCC-structured HEAs are resistant to irradiation hardening, their phase stability under irradiation conditions remains a key issue. The second phase precipitated by phase instability can serve as the recombination core of annihilation, thus inhibiting the formation and growth of helium bubbles. An interface between the precipitated phase and the matrix, especially the substructure interface, can lead to the formation, accumulation, and nucleation of lattice defects, thus inducing hardening embrittlement and other ion-induced damage, and its effects need to be further studied. RHEAs have been considered for use in irradiation conditions due to their high melting points and potentially superior radiation damage resistance. However, several challenges arise when they are exposed to such harsh environments:

1. Radiation-induced phase segregation and precipitation: RHEAs may experience changes in the microstructure due to radiation, including segregation of elements and precipitation of new phases, which can change their mechanical properties and lead to embrittlement or reduced strength.
2. Swelling and void formation: exposure to irradiation can lead to the formation of voids and swelling in the material, which can damage the integrity of the material's structure and lead to premature failure of the alloy under mechanical stress.
3. Helium embrittlement: Transmutation reactions within nuclear reactors can lead to the formation of helium or helium bubbles within the alloy. These helium bubbles create pressure within the material, leading to embrittlement and cracking.
4. Long-term behavior: The long-term behavior of RHEAs under irradiation is not fully understood, making it difficult to predict their performance over the lifespan of a nuclear reactor. This uncertainty can be a significant barrier to their adoption in safety-critical applications.
5. Irradiation-induced changes in other properties: Irradiation can lead to variation in the microstructure of RHEAs, thus resulting in changes in other properties, such as damping, armoring, corrosion and oxidation resistance, thermal expansion, etc. On the one hand, the study of the variation in these properties is a necessary part of the comprehensive evaluation of RHEAs under irradiation conditions; on the other hand, it can also broaden the range and possibility of their applications. However, research in these fields has rarely been reported.

5. Future Prospects

As a future direction in materials science and nuclear engineering, it is suggested that researchers focus on optimizing alloy compositions continuously and refine post-irradiation heat treatments to effectively manage radiation-induced segregation and precipitation. This involves tailoring alloys to stabilize the desired phases and minimize detrimental secondary phases, as well as utilizing heat treatments to re-dissolve segregated elements and eliminate unwanted precipitates.

The swelling and void problem can be solved by the incorporation of alloying strategies with elements known to form stable oxides or nitrides. This can be explored to effectively restrain dislocations and inhibit void formation in radiation-exposed materials.

One promising approach to addressing helium embrittlement in future research is to focus on the creation of effective helium trapping sites within materials. This can be achieved by incorporating specific microstructural features, such as finely dispersed oxides or carbides, which have the capability to capture and immobilize helium atoms. Additionally, the design of dual-phase alloys is another future direction. By engineering alloys with one phase that is more resistant to helium embrittlement, it becomes possible to maintain the overall ductility and integrity of the material, even in helium-rich environments. These strategies hold the potential to advance the development of materials for nuclear reactors and aerospace technology.

Due to the predominance of short-duration irradiation experiments in laboratory settings, there exists a necessity to delve into the long-term behavioral responses of materials within irradiation environments. Irradiation experiments with extended exposure durations can simultaneously collect data related to material evolution under irradiation. Moreover, irradiation-induced changes in other properties of RHEAs, i.e., damping, armoring, corrosion and oxidation resistance, and thermal expansion, are worth further study. Furthermore, the enhancement of computational models holds great potential. This entails the refinement of predictive frameworks, encompassing multiscale modeling methodologies that enable the prediction of long-term material behavior under irradiation. Such models should include effects ranging from the atomic scale to the macroscopic scale, contributing to a more comprehensive understanding of radiation-induced material alterations over extended periods.

Author Contributions: Conceptualization, C.Y.; validation, B.S. and D.S.; writing—original draft preparation, B.W.; writing—review and editing, C.Y.; supervision, D.S. and B.S. All authors have read and agreed to the published version of the manuscript.

Funding: The authors gratefully acknowledge the financial support of the National Natural Science Foundation of China (nos. 51821001 and 52090042) and the Science and Technology Cooperation Project of Inner Mongolia Autonomous Region and Shanghai Jiao Tong University (no. 2023XYJG0001-01-01).

Data Availability Statement: Not applicable.

Conflicts of Interest: The authors declare no conflict of interest.

References

1. Pioro, I.L.; Rodriguez, G.H. Generation IV International Forum (GIF). In *Handbook of Generation IV Nuclear Reactors*; Elsevier: Amsterdam, The Netherlands, 2023; pp. 111–132.
2. Patel, D.; Richardson, M.D.; Jim, B.; Akhmadaliev, S.; Goodall, R.; Gandy, A.S. Radiation Damage Tolerance of a Novel Metastable Refractory High Entropy Alloy V_{2.5}Cr_{1.2}WMoCo_{0.04}. *J. Nucl. Mater.* **2020**, *531*, 152005. [[CrossRef](#)]
3. Shen, S.; Chen, F.; Tang, X.; Lin, J.; Ge, G.; Liu, J. Effects of Carbon Doping on Irradiation Resistance of Fe₃₈Mn₄₀Ni₁₁Al₄Cr₇ High Entropy Alloys. *J. Nucl. Mater.* **2020**, *540*, 152380. [[CrossRef](#)]
4. Sadeghilardjani, M.; Ayyagari, A.; Muskeri, S.; Hasannaeimi, V.; Salloom, R.; Chen, W.-Y.; Mukherjee, S. Ion Irradiation Response and Mechanical Behavior of Reduced Activity High Entropy Alloy. *J. Nucl. Mater.* **2020**, *529*, 151955. [[CrossRef](#)]
5. Fang, Q.; Peng, J.; Chen, Y.; Li, L.; Feng, H.; Li, J.; Jiang, C.; Liaw, P.K. Hardening Behaviour in the Irradiated High Entropy Alloy. *Mech. Mater.* **2021**, *155*, 103744. [[CrossRef](#)]
6. Ivanov, I.A.; Ryskulov, A.; Kurakhmedov, A.; Kozlovskiy, A.; Shlimas, D.; Zdorovets, M.V.; Uglov, V.V.; Zlotski, S.V.; Ke, J. Radiation Swelling and Hardness of High-Entropy Alloys Based on the TiTaNbV System Irradiated with Krypton Ions. *J. Mater. Sci. Mater. Electron.* **2021**, *32*, 27260–27267. [[CrossRef](#)]
7. Shi, T.; Su, Z.; Li, J.; Liu, C.; Yang, J.; He, X.; Yun, D.; Peng, Q.; Lu, C. Distinct Point Defect Behaviours in Body-Centred Cubic Medium-Entropy Alloy NbZrTi Induced by Severe Lattice Distortion. *Acta Mater.* **2022**, *229*, 117806. [[CrossRef](#)]
8. Pu, G.; Sun, S.; Wang, S.; Gan, L.; Chen, S.; Ye, Z.; Huang, Z.; Zheng, J.; Wang, Z.; Yang, C.; et al. A Comparative Study of Irradiation Response in Amorphous TaTiWVCr Refractory High Entropy Alloy with the Counterpart of Tungsten Films. *Intermetallics* **2023**, *156*, 107850. [[CrossRef](#)]
9. Chen, D.; Zhao, S.; Sun, J.; Tai, P.; Sheng, Y.; Zhao, Y.; Yeli, G.; Lin, W.; Liu, S.; Kai, W.; et al. Diffusion Controlled Helium Bubble Formation Resistance of FeCoNiCr High-Entropy Alloy in the Half-Melting Temperature Regime. *J. Nucl. Mater.* **2019**, *526*, 151747. [[CrossRef](#)]
10. Sturcken, E.F. Irradiation Effects in Magnesium and Aluminum Alloys. *J. Nucl. Mater.* **1979**, *82*, 39–53. [[CrossRef](#)]
11. Hou, Y.; Li, D.; Lu, Y.; Huang, H.; Yang, W.; Liu, R. Xe Ion Irradiation-Induced Microstructural Evolution and Hardening Effect of Nickel-Base Superalloy. *Sci. Technol. Nucl. Install.* **2021**, *2021*, 5535478. [[CrossRef](#)]
12. Feng, J.; Zhang, X.; Chu, Y.; Wan, J. Hydrogen Embrittlement of Ni-Based Superalloy Inconel 625 Fabricated by Wire Arc Additive Manufacturing: The Role of Laves Phase. *Met. Mater. Int.* **2023**. [[CrossRef](#)]
13. Lu, X.; Ma, Y.; Wang, D. On the Hydrogen Embrittlement Behavior of Nickel-Based Alloys: Alloys 718 and 725. *Mater. Sci. Eng. A* **2020**, *792*, 139785. [[CrossRef](#)]
14. Steinbrück, M. Hydrogen Absorption by Zirconium Alloys at High Temperatures. *J. Nucl. Mater.* **2004**, *334*, 58–64. [[CrossRef](#)]
15. Motta, A.T.; Capolungo, L.; Chen, L.-Q.; Cinbiz, M.N.; Daymond, M.R.; Koss, D.A.; Lacroix, E.; Pastore, G.; Simon, P.-C.A.; Tonks, M.R.; et al. Hydrogen in Zirconium Alloys: A Review. *J. Nucl. Mater.* **2019**, *518*, 440–460. [[CrossRef](#)]

16. Shin, J.H.; Kong, B.S.; Jeong, C.; Eom, H.J.; Jang, C.; AlMousa, N.; Woller, K.B.; Short, M.P. Swelling Resistance of an Austenitic Stainless Steel with Uniformly Distributed Nanosized NbC Precipitates under Heavy Ion Irradiation. *J. Nucl. Mater.* **2022**, *564*, 153678. [[CrossRef](#)]
17. Was, G.S.; Wharry, J.P.; Frisbie, B.; Wirth, B.D.; Morgan, D.; Tucker, J.D.; Allen, T.R. Assessment of Radiation-Induced Segregation Mechanisms in Austenitic and Ferritic–Martensitic Alloys. *J. Nucl. Mater.* **2011**, *411*, 41–50. [[CrossRef](#)]
18. Dong, Z.; Ma, Z.; Yu, L.; Liu, Y. Achieving High Strength and Ductility in ODS-W Alloy by Employing oxide@W Core-Shell Nanopowder as Precursor. *Nat. Commun.* **2021**, *12*, 5052. [[CrossRef](#)]
19. Oñoro, M.; Macías-Delgado, J.; Auger, M.A.; De Castro, V.; Leguey, T. Mechanical Properties and Stability of Precipitates of an ODS Steel after Thermal Cycling and Aging. *Nucl. Mater. Energy* **2020**, *24*, 100758. [[CrossRef](#)]
20. Murty, K.L.; Charit, I. Structural Materials for Gen-IV Nuclear Reactors: Challenges and Opportunities. *J. Nucl. Mater.* **2008**, *383*, 189–195. [[CrossRef](#)]
21. Odette, G.R.; Zinkle, S.J. Structural Alloys for Nuclear Energy Applications. In *Structural Alloys for Nuclear Energy Applications*; Elsevier: Amsterdam, The Netherlands, 2019.
22. Allen, T.; Busby, J.; Meyer, M.; Petti, D. Materials Challenges for Nuclear Systems. *Mater. Today* **2010**, *13*, 14–23. [[CrossRef](#)]
23. Wen, C.; Wang, C.; Zhang, Y.; Antonov, S.; Xue, D.; Lookman, T.; Su, Y. Modeling Solid Solution Strengthening in High Entropy Alloys Using Machine Learning. *Acta Mater.* **2021**, *212*, 116917. [[CrossRef](#)]
24. Miracle, D.B.; Senkov, O.N. A Critical Review of High Entropy Alloys and Related Concepts. *Acta Mater.* **2017**, *122*, 448–511. [[CrossRef](#)]
25. Lu, C.; Jin, K.; Béland, L.K.; Zhang, F.; Yang, T.; Qiao, L.; Zhang, Y.; Bei, H.; Christen, H.M.; Stoller, R.E.; et al. Direct Observation of Defect Range and Evolution in Ion-Irradiated Single Crystalline Ni and Ni Binary Alloys. *Sci. Rep.* **2016**, *6*, 19994. [[CrossRef](#)] [[PubMed](#)]
26. Jin, K.; Lu, C.; Wang, L.M.; Qu, J.; Weber, W.J.; Zhang, Y.; Bei, H. Effects of Compositional Complexity on the Ion-Irradiation Induced Swelling and Hardening in Ni-Containing Equiatomic Alloys. *Scr. Mater.* **2016**, *119*, 65–70. [[CrossRef](#)]
27. He, M.R.; Wang, S.; Jin, K.; Bei, H.; Yasuda, K.; Matsumura, S.; Higashida, K.; Robertson, I.M. Enhanced Damage Resistance and Novel Defect Structure of CrFeCoNi under in Situ Electron Irradiation. *Scr. Mater.* **2016**, *125*, 5–9. [[CrossRef](#)]
28. Chen, W.Y.; Liu, X.; Chen, Y.; Yeh, J.W.; Tseng, K.K.; Natesan, K. Irradiation Effects in High Entropy Alloys and 316H Stainless Steel at 300 °C. *J. Nucl. Mater.* **2018**, *510*, 421–430. [[CrossRef](#)]
29. Wang, X.; Jin, K.; Chen, D.; Bei, H.; Wang, Y.; Weber, W.J.; Zhang, Y.; More, K.L. Effects of Fe Concentration on Helium Bubble Formation in NiFex Single-Phase Concentrated Solid Solution Alloys. *Materialia* **2019**, *5*, 100183. [[CrossRef](#)]
30. Cui, H.; Liu, N.; Luo, L.; Xu, Y.; Cheng, J.; Wu, Y. Behavior of High-Entropy W-Rich Alloys $W_x(TaVCrTi)_y$ under He^+ Irradiation. *Fusion Eng. Des.* **2021**, *172*, 112904. [[CrossRef](#)]
31. Chang, S.; Tseng, K.K.; Yang, T.Y.; Chao, D.S.; Yeh, J.W.; Liang, J.H. Irradiation-Induced Swelling and Hardening in $HfNbTaTiZr$ Refractory High-Entropy Alloy. *Mater. Lett.* **2020**, *272*, 127832. [[CrossRef](#)]
32. Ma, N.; Liu, S.; Liu, W.; Xie, L.; Wei, D.; Wang, L.; Li, L.; Zhao, B.; Wang, Y. Research Progress of Titanium-Based High Entropy Alloy: Methods, Properties, and Applications. *Front. Bioeng. Biotechnol.* **2020**, *8*, 603522. [[CrossRef](#)]
33. Zhang, Y.; Fang, S.; Wang, Y.; Zhang, D. Enhancement of Tensile Strength and Ductility of Titanium with a Bimodal Structure. *Mater. Sci. Eng. A* **2021**, *803*, 140701. [[CrossRef](#)]
34. Lo, K.-C.; Chang, Y.-J.; Murakami, H.; Yeh, J.-W.; Yeh, A.-C. An Oxidation Resistant Refractory High Entropy Alloy Protected by $CrTaO_4$ -Based Oxide. *Sci. Rep.* **2019**, *9*, 7266. [[CrossRef](#)] [[PubMed](#)]
35. Gawel, R.; Rogal, L.; Grzesik, Z. Behaviour of Al, Co, Cr, Ni-Based High Entropy Alloys under High-Temperature Thermal Shock Oxidising Conditions. *Corros. Sci.* **2022**, *198*, 110116. [[CrossRef](#)]
36. Chen, T.; Shi, Y.; Ren, Y.; Li, X.; Liu, Z.; Han, T. Effect of Cr Content on Synergistic Effect of Cr-Al during Oxidation of High-Entropy AlCoCr_xNiTi Alloys. *Corros. Sci.* **2024**, *227*, 111690. [[CrossRef](#)]
37. Shusterman, J.A.; Scielzo, N.D.; Thomas, K.J.; Norman, E.B.; Lapi, S.E.; Loveless, C.S.; Peters, N.J.; Robertson, J.D.; Shaughnessy, D.A.; Tonchev, A.P. The Surprisingly Large Neutron Capture Cross-Section of ^{88}Zr . *Nature* **2019**, *565*, 328–330. [[CrossRef](#)] [[PubMed](#)]
38. Xiang, C.; Han, E.-H.; Zhang, Z.M.; Fu, H.M.; Wang, J.Q.; Zhang, H.F.; Hu, G.D. Design of Single-Phase High-Entropy Alloys Composed of Low Thermal Neutron Absorption Cross-Section Elements for Nuclear Power Plant Application. *Intermetallics* **2019**, *104*, 143–153. [[CrossRef](#)]
39. Xu, J.; Li, H.; Zhao, X.; Wu, J.; Zhao, B.; Zhao, H.; Wu, J.; Zhang, Y.; Liu, C. Zirconium Based Neutron Absorption Material with Outstanding Corrosion Resistance and Mechanical Properties. *J. Nucl. Mater.* **2022**, *567*, 153763. [[CrossRef](#)]
40. Periodic Table of Elements: Sorted by Cross Section (Thermal Neutron Capture) (EnvironmentalChemistry.Com). Available online: <https://environmentalchemistry.com/yogi/periodic/crosssection.html> (accessed on 29 November 2023).
41. El-Atwani, O.; Li, N.; Li, M.; Devaraj, A.; Baldwin, J.K.S.; Schneider, M.M.; Sobieraj, D.; Wróbel, J.S.; Nguyen-Manh, D.; Maloy, S.A.; et al. Outstanding Radiation Resistance of Tungsten-Based High-Entropy Alloys. *Sci. Adv.* **2019**, *5*, eaav2002. [[CrossRef](#)]
42. Wang, P.; Li, M.; Malomo, B.; Yang, L. Lattice Distortion and Re-Distortion Affecting Irradiation Tolerance in High Entropy Alloys. *Nanoscale* **2023**, *15*, 16447–16457. [[CrossRef](#)]

43. El Atwani, O.; Vo, H.T.; Tunes, M.A.; Lee, C.; Alvarado, A.; Krienke, N.; Poplawsky, J.D.; Kohnert, A.A.; Gigax, J.; Chen, W.-Y.; et al. A Quinary WTaCrVHF Nanocrystalline Refractory High-Entropy Alloy Withholding Extreme Irradiation Environments. *Nat. Commun.* **2023**, *14*, 2516. [[CrossRef](#)]
44. Doppelstein, H.; George, E.P.; Gurevich, E.L.; Kostka, A.; Ostendorf, A.; Laplanche, G. Laser Metal Deposition of Refractory High-Entropy Alloys for High-Throughput Synthesis and Structure-Property Characterization. *Int. J. Extreme Manuf.* **2020**, *3*, 015201. [[CrossRef](#)]
45. Cheng, W.; Ji, L.; Zhang, L.; Wang, H.; Sun, W. Refractory High-Entropy Alloys Fabricated Using Laser Technologies: A Concrete Review. *J. Mater. Res. Technol.* **2023**, *24*, 7497–7524. [[CrossRef](#)]
46. Ren, X.; Li, Y.; Qi, Y.; Wang, B. Review on Preparation Technology and Properties of Refractory High Entropy Alloys. *Materials* **2022**, *15*, 2931. [[CrossRef](#)] [[PubMed](#)]
47. Nagase, T.; Mizuchi, K.; Nakano, T. Solidification Microstructures of the Ingots Obtained by Arc Melting and Cold Crucible Levitation Melting in TiNbTaZr Medium-Entropy Alloy and TiNbTaZrX (X = V, Mo, W) High-Entropy Alloys. *Entropy* **2019**, *21*, 483. [[CrossRef](#)] [[PubMed](#)]
48. Xiong, W.; Guo, A.X.Y.; Zhan, S.; Liu, C.-T.; Cao, S.C. Refractory High-Entropy Alloys: A Focused Review of Preparation Methods and Properties. *J. Mater. Sci. Technol.* **2023**, *142*, 196–215. [[CrossRef](#)]
49. Neutron Scattering Lengths and Cross Sections. Available online: <https://www.ncnr.nist.gov/resources/n-lengths/list.html> (accessed on 29 November 2023).
50. Periodic Table—Royal Society of Chemistry. Available online: <https://www.rsc.org/periodic-table> (accessed on 29 November 2023).
51. Pickering, E.J.; Carruthers, A.W.; Barron, P.J.; Middleburgh, S.C.; Armstrong, D.E.J.; Gandy, A.S. High-Entropy Alloys for Advanced Nuclear Applications. *Entropy* **2021**, *23*, 98. [[CrossRef](#)]
52. Kumar, N.A.P.K.; Li, C.; Leonard, K.J.; Bei, H.; Zinkle, S.J. Microstructural Stability and Mechanical Behavior of FeNiMnCr High Entropy Alloy under Ion Irradiation. *Acta Mater.* **2016**, *113*, 230–244. [[CrossRef](#)]
53. Kareer, A.; Waite, J.C.; Li, B.; Couet, A.; Armstrong, D.E.J.; Wilkinson, A.J. Short Communication: ‘Low Activation, Refractory, High Entropy Alloys for Nuclear Applications’. *J. Nucl. Mater.* **2019**, *526*, 151744. [[CrossRef](#)]
54. Moschetti, M.; Xu, A.; Schuh, B.; Hohenwarter, A.; Couzinié, J.-P.; Kružic, J.J.; Bhattacharyya, D.; Gludovatz, B. On the Room-Temperature Mechanical Properties of an Ion-Irradiated TiZrNbHfTa Refractory High Entropy Alloy. *JOM* **2020**, *72*, 130–138. [[CrossRef](#)]
55. Moschetti, M.; Xu, A.; Hohenwarter, A.; Wei, T.; Davis, J.; Short, K.; Thorogood, G.J.; Kong, C.; Couzinié, J.-P.; Bhattacharyya, D.; et al. The Influence of Phase Formation on Irradiation Tolerance in a Nanocrystalline TiZrNbHfTa Refractory High-Entropy Alloy. *Adv. Eng. Mater.* **2023**, *23*, 00863. [[CrossRef](#)]
56. Zong, Y.; Hashimoto, N.; Oka, H. Study on Irradiation Effects of Refractory Bcc High-Entropy Alloy. *Nucl. Mater. Energy* **2022**, *31*, 101158. [[CrossRef](#)]
57. Corbett, J.W. Radiation-induced voids in metals. In Proceedings of the 1971 International Conference, Albany, NY, USA, 9–11 June 1971.
58. Okamoto, P.R.; Rehn, L.E. Radiation-Induced Segregation in Binary and Ternary Alloys. *J. Nucl. Mater.* **1979**, *83*, 2–23. [[CrossRef](#)]
59. Tunes, M.A.; Vo, H.T.; Baldwin, J.K.S.; Saleh, T.A.; Fensin, S.J.; El-Atwani, O. Perspectives on Novel Refractory Amorphous High-Entropy Alloys in Extreme Environments. *Appl. Mater. Today* **2023**, *32*, 101796. [[CrossRef](#)]
60. Li, T.; Lu, Y.; Cao, Z.; Wang, T.; Li, T. Opportunity and Challenge of Refractory High-Entropy Alloys in the Field of Reactor Structural Materials. *Jinshu Xuebao Acta Met. Sin.* **2021**, *57*, 42–54. [[CrossRef](#)]
61. Hu, Y.; Liu, X.; Guo, N.; Wang, L. Microstructure and Mechanical Properties of NbZrTi and NbHfZrTi Alloys. *Rare Met.* **2019**, *38*, 840–847. [[CrossRef](#)]
62. Wu, Y.D.; Cai, Y.H.; Wang, T.; Si, J.J.; Zhu, J.; Wang, Y.D.; Hui, X.D. A Refractory Hf₂₅Nb₂₅Ti₂₅Zr₂₅ High-Entropy Alloy with Excellent Structural Stability and Tensile Properties. *Mater. Lett.* **2014**, *130*, 277–280. [[CrossRef](#)]
63. Senkov, O.N.; Scott, J.M.; Senkova, S.V.; Miracle, D.B.; Woodward, C.F. Microstructure and Room Temperature Properties of a High-Entropy TaNbHfZrTi Alloy. *J. Alloys Compd.* **2011**, *509*, 6043–6048. [[CrossRef](#)]
64. Senkov, O.N.; Scott, J.M.; Senkova, S.V.; Meisenkothen, F.; Miracle, D.B.; Woodward, C.F. Microstructure and Elevated Temperature Properties of a Refractory TaNbHfZrTi Alloy. *J. Mater. Sci.* **2012**, *47*, 4062–4074. [[CrossRef](#)]
65. Jia, Y.; Zhang, L.; Li, P.; Ma, X.; Xu, L.; Wu, S.; Jia, Y. Microstructure and Mechanical Properties of Nb–Ti–V–Zr Refractory Medium-Entropy Alloys. *Front. Mater.* **2020**, *7*, 172. [[CrossRef](#)]
66. Wu, Y.D.; Cai, Y.H.; Chen, X.H.; Wang, T.; Si, J.J.; Wang, L.; Wang, Y.D.; Hui, X.D. Phase Composition and Solid Solution Strengthening Effect in TiZrNbMoV High-Entropy Alloys. *Mater. Des.* **2015**, *83*, 651–660. [[CrossRef](#)]
67. Su, Y.; Xia, S.; Huang, J.; Liu, Q.; Liu, H.; Wang, C.; Wang, Y. Irradiation Behaviors in BCC Multi-Component Alloys with Different Lattice Distortions. *Metals* **2021**, *11*, 706. [[CrossRef](#)]
68. Lei, Z.; Wu, Y.; He, J.; Liu, X.; Wang, H.; Jiang, S.; Gu, L.; Zhang, Q.; Gault, B.; Raabe, D.; et al. Snoek-Type Damping Performance in Strong and Ductile High-Entropy Alloys. *Sci. Adv.* **2020**, *6*, eaba7802. [[CrossRef](#)] [[PubMed](#)]
69. Egami, T.; Guo, W.; Rack, P.D.; Nagase, T. Irradiation Resistance of Multicomponent Alloys. *Met. Mater. Trans. A* **2014**, *45*, 180–183. [[CrossRef](#)]

70. Caturla, M.J.; Diaz De La Rubia, T.; Fluss, M. Modeling Microstructure Evolution of f.c.c. Metals under Irradiation in the Presence of He. *J. Nucl. Mater.* **2003**, *323*, 163–168. [[CrossRef](#)]
71. Zinkle, S.J.; Snead, L.L. Designing Radiation Resistance in Materials for Fusion Energy. *Annu. Rev. Mater. Res.* **2014**, *44*, 241–267. [[CrossRef](#)]
72. Jia, N.; Li, Y.; Huang, H.; Chen, S.; Li, D.; Dou, Y.; He, X.; Yang, W.; Xue, Y.; Jin, K. Helium Bubble Formation in Refractory Single-Phase Concentrated Solid Solution Alloys under MeV He Ion Irradiation. *J. Nucl. Mater.* **2021**, *550*, 152937. [[CrossRef](#)]
73. Guo, Y.; Zhang, P.; Zhang, X.; Cui, Y.; Mei, X.; Li, X.; Fan, H.; Liu, D.; Wang, Y. Study on the Microstructural Evolution in NbMoTaW Series Refractory Multi-Principal Element Alloy Films by Low-Energy and High-Flux He Ions Irradiation. *Surf. Coat. Technol.* **2023**, *452*, 129140. [[CrossRef](#)]
74. Senkov, O.N.; Wilks, G.B.; Miracle, D.B.; Chuang, C.P.; Liaw, P.K. Refractory High-Entropy Alloys. *Intermetallics* **2010**, *18*, 1758–1765. [[CrossRef](#)]
75. Zhang, Z.; Han, E.H.; Xiang, C. Irradiation Behaviors of Two Novel Single-Phase Bcc-Structure High-Entropy Alloys for Accident-Tolerant Fuel Cladding. *J. Mater. Sci. Technol.* **2021**, *84*, 230–238. [[CrossRef](#)]
76. Lu, Y.; Huang, H.; Gao, X.; Ren, C.; Gao, J.; Zhang, H.; Zheng, S.; Jin, Q.; Zhao, Y.; Lu, C.; et al. A Promising New Class of Irradiation Tolerant Materials: $Ti_2ZrHfV_{0.5}Mo_{0.2}$ High-Entropy Alloy. *J. Mater. Sci. Technol.* **2019**, *35*, 369–373. [[CrossRef](#)]

Disclaimer/Publisher's Note: The statements, opinions and data contained in all publications are solely those of the individual author(s) and contributor(s) and not of MDPI and/or the editor(s). MDPI and/or the editor(s) disclaim responsibility for any injury to people or property resulting from any ideas, methods, instructions or products referred to in the content.